Surface instability of confined elastic bilayers: Theory and simulations

Gaurav Tomar,[1] Ashutosh Sharma,[2,*] Vijay Shenoy,[3] and Gautam Biswas[1]
[1]*Department of Mechanical Engineering, Indian Institute of Technology, Kanpur, UP 208016, India*
[2]*Department of Chemical Engineering, Indian Institute of Technology, Kanpur, UP 208016, India*
[3]*Materials Research Center and Center for Condensed Matter Theory, Indian Institute of Science, Bangalore, 560012, India*
(Received 13 September 2006; revised manuscript received 15 April 2007; published 30 July 2007)

The surface of a soft elastic film becomes unstable and forms a self-organized undulating pattern because of adhesive interactions when it comes in contact proximity with a rigid surface. For a single film, the pattern length scale λ, which is governed by the minimization of the elastic stored energy, gives $\lambda \sim 3h$, where h is the film thickness. Based on a linear stability analysis and simulations of adhesion and debonding, we consider the contact instability of an elastic bilayer, which provides greater flexibility in the morphological control of interfacial instability. Unlike the case of a single film, the morphology of the contact instability patterns, debonding distance, and debonding force in a bilayer can be controlled in a nonlinear way by varying the thicknesses and shear moduli of the films. Interestingly, the pattern wavelength in a bilayer can be greatly increased or decreased compared to a single film when the adhesive contact is formed by the stiffer or the softer of the two films, respectively. In particular, λ as small as $0.5h$ can be obtained. This indicates a new strategy for pattern miniaturization in elastic contact lithography.

DOI: 10.1103/PhysRevE.76.011607 PACS number(s): 68.35.Gy, 68.35.Np, 05.65.+b

I. INTRODUCTION

The surface of a soft elastic film undergoes spontaneous surface roughening when it comes in adhesive contact with another surface [1–16]. Instability at the surface is initiated when the adhesive interaction (van der Waals, electrostatic, etc.) between the film surface and the approaching surface exceeds the minimum of the stabilizing elastic force. Interestingly, the wavelength of the elastic contact instability in a soft elastic film is theoretically predicted and experimentally verified to be independent of the nature of interactions between the surfaces [2,4,5,8–15,17]. This is because the selected wavelength beyond the critical force is based solely on the minimum of the elastic stored energy. Moreover, the wavelength of the elastic contact instability patterns in films thicker than about 1 μm is linearly proportional to the thickness of the film, $\lambda \sim 3h$ [4,5,8,11–15]. This is in contrast to the instabilities in thin liquid films where the precise nature and magnitude of external forces determine the length scale and morphology of the instability [18–24]. The interfacial instability of elastic surface layers on thin viscous films have also been investigated [25–27]. Elastic layers can also readily self-organize under interfacial tension gradients [28] and wetting interactions [29]. Finally, it may be noted that the surface energy effects also become important in submicrometer-thickness elastic films [15], as well as in a semi-infinite elastic film [9]—in the former case, because of its high surface to volume ratio, and in the latter case, because of the lack of any other stabilizing factor. We consider here the case of intermediate-thickness films of most practical interest where the surface tension effects can be neglected.

The self-organized contact instability in a single soft elastic film of constant shear modulus has been extensively studied [2,4,5,7–15,17], both theoretically and experimentally, because of its importance in the understanding of confinement effects, spontaneous pattern formation, adhesion, friction, and debonding at soft interfaces and its potential application in mesopatterning [30,31]. However, the instability length scale in a single film thicker than about 1 μm is controlled entirely by the film thickness, regardless of its elastic properties [8,11,12,15]. A greater control on the interfacial morphology would be helpful for self-organized mesopatterning and engineering of optimal pressure-sensitive adhesives. We show here that additional flexibility and controls can indeed be introduced by considering a bilayer of two different thickness and shear moduli. In particular, we show that under appropriate conditions, it becomes possible to reduce the pattern wavelength to be even smaller than the total bilayer thickness. This is in contrast to a single elastic film which always exhibits a pattern wavelength of $\sim 3h$. Also, in many applications of surface-cured adhesives, layered composites, and biosurfaces, bilayers are a more appropriate model of a variable property film. A bilayer system is also of practical interest [32–34] in situations where a softer coating is deposited on a stiffer film in order to prevent severe indentation or when a harder surface layer is glued to a soft elastic film in order to achieve a cleaner separation of adhesive layers. Although the surface instability caused by the interactions between two elastic films bonded to two different substrates has been fully analyzed [35–38], the surface instability of an elastic bilayer has only recently started to be addressed by a linear stability analysis [39]. The linear analysis in Ref. [39] was based on a Kerr-type [40] approximate differential relation relating surface normal stress to the surface normal displacement at the free surface. An interesting conclusion is the possibility of two competing wavelengths for the instability, rather than a single length scale as in a single-film problem. This phenomenon has similar physical origins as in the problem of two separate elastic films interacting with each other [35–38].

*Author to whom correspondence should be addressed. ashutos@iitk.ac.in

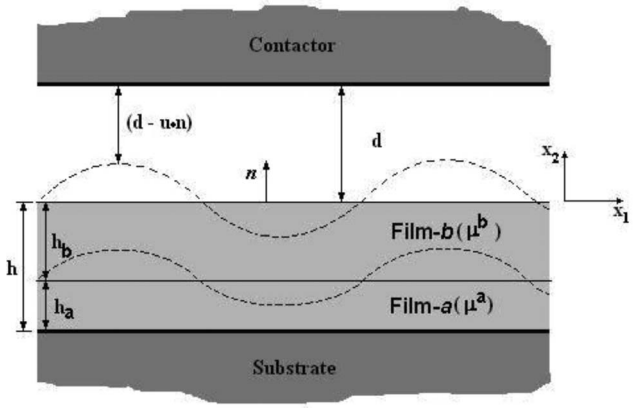

FIG. 1. A thin elastic bilayer film bonded rigidly to a substrate interacting with a contactor. The dashed lines show possible deformed configuration of the bilayer system.

The approach developed here is based on a formulation suitable for both the linear stability analysis and the energy minimization used for simulations. In the present study, the surface instability as well as debonding characteristics of an elastic-bilayer system interacting with a rigid contacting surface is considered based on a general formalism used previously for the analysis of a single elastic film [5,8], which was also applied to the contact problem of two separate films [36,37]. The results for both situations of interest, the surface layer being stiffer or softer than the base layer, are considered. In addition to the linear stability analysis valid at the onset of instability during the initial adhesion phase, simulations are carried out to study the debonding process during the pull-off. The simulations of elastic bilayer debonding starting from adhesive contact are based on the search for locally stable surface morphologies corresponding to the local energy minima [8,11,12,15]. The paper is organized as follows. Formulation and governing equations for the system considered (Fig. 1) are presented in Sec. II. Linear stability analysis (LSA) results are discussed in Sec. III. Results from the simulations are presented in Sec. IV, and the key conclusions from the present study are summarized in Sec. V.

II. FORMULATION

The system under investigation is shown schematically in Fig. 1. The elastic film a is bonded rigidly to a substrate and the interface between the two films is slip free. Film a and film b have constant shear moduli μ^a and μ^b, respectively. Both films in this study are considered to be incompressible. The mean separation distance between the free surface of the top film b and the contactor is denoted by d. When the distance d becomes less than a critical distance d_c, the long-range van der Waals attractive force and, possibly, the electrostatic attractive interaction induce the film to undergo inhomogeneous deformations and lose planarity. The dashed lines in Fig. 1 show a schematic of this event. The normal unit vector at the free surface of film b is $\boldsymbol{n}$. A coordinate system (x_1, x_2) with positive x_2 along the outward normal of the free surface is used to describe the position vectors.

The total potential energy (Π) of the system is given by the sum of the stored elastic energies of the two films and the intersurface adhesive interaction energy:

$$\Pi = \int_V W(\boldsymbol{\varepsilon}) dV - \int_{S^b} U(d - \boldsymbol{u}^b \cdot \boldsymbol{n}) dS^b, \tag{1}$$

where ε is the strain tensor and W is the strain energy density of the system given by

$$W(\boldsymbol{\varepsilon}) = \begin{cases} \dfrac{\mu^a}{2} \boldsymbol{\varepsilon}:\boldsymbol{\varepsilon} \text{ in film } a, \\ \dfrac{\mu^b}{2} \boldsymbol{\varepsilon}:\boldsymbol{\varepsilon} \text{ in film } b. \end{cases} \tag{2}$$

Here, $\boldsymbol{u}^b$ is the displacement vector of the free surface of film b, V denotes the total volume of the films, and S^b is the free surface area of film b. The function U represents the adhesive interaction energy per unit area.

A generic adhesive interaction potential U used here for the linear stability analysis can be expanded in power series about the reference state of the undeformed film. Retaining the terms to second order,

$$U(d - \boldsymbol{u}^b \cdot \boldsymbol{n}) \approx U_0 + F(\boldsymbol{u}^b \cdot \boldsymbol{n}) + \frac{1}{2} Y(\boldsymbol{u}^b \cdot \boldsymbol{n})^2, \tag{3}$$

where,

$$U_0 = U(d), \quad F = U'(d), \quad Y = U''(d). \tag{4}$$

The form Y has dimensions of force per unit volume and is termed the *interaction stiffness*. Similarly, F is the interaction force per unit area (analogous to pressure). Substituting the above form of the potential [Eq. (3)] into Eq. (1), one obtains the following expression for the total energy, which is used to carry out the linear stability analysis:

$$\Pi_a = \int_V W(\boldsymbol{\varepsilon}) dV - \int_{S^b} \left(U_0 + F(\boldsymbol{u}^b \cdot \boldsymbol{n}) + \frac{1}{2} Y(\boldsymbol{u}^b \cdot \boldsymbol{n})^2 \right) dS^b. \tag{5}$$

The minimum of the total potential energy corresponds to the equilibrium displacement field which satisfies the following boundary conditions. Normal and shear stresses are continuous at the common interface of the two constituent films of the bilayer film. Also, the displacement field is continuous at the common interface. The bottom surface of the film a is bonded rigidly to the substrate. The free surface of film b is assumed to be shear free. The inclusion of coupled tension-shear interactions does not introduce new physics or greatly alter the numerical prefactor for the wavelength [6]. The normal stress balance at the free surface yields

$$\sigma_{22}^b = F + (u_2^b) Y, \tag{6}$$

where σ_{22}^b is the normal stress component of the stress tensor (σ_{ij}) at the free surface.

III. STABILITY ANALYSIS

In this section, we perform the linear stability analysis by perturbing the homogeneous flat interfaces with normal linear modes. We consider plane strain approximation in the formulation and neglect the variations in the x_3 direction. Incompressibility of the films leads to a homogeneous strain-free field and, consequently, the stress field is that of constant pressure equal to F given in Eq. (6).

The displacement field in both films is governed by the stress equilibrium equation ($\nabla \cdot \boldsymbol{\sigma}=0$), which can be written as (using a linear constitutive stress-strain relation)

$$p_{,i} + \mu u_{i,jj} = 0,$$

where

$$\mu = \mu^a, \quad \text{in film } a, \quad \mu = \mu^b, \quad \text{in film } b, \tag{7}$$

together with the incompressibility condition

$$\nabla \cdot \boldsymbol{u} = 0. \tag{8}$$

The perturbed displacement and pressure field in films a and b for any arbitrary wave number k are now assumed to be

$$u_i^{a,b} = \tilde{u}_i^{a,b}(x_2)e^{ikx_1} \quad \text{for } i = 1,2, \tag{9}$$

$$p^{a,b} = \tilde{p}^{a,b}(x_2)e^{ikx_1}. \tag{10}$$

Substituting the perturbed field into Eqs. (8) and (9), we obtain a set of biharmonic equations

$$\frac{d^4\tilde{u}_2^a}{dx_2^4} - 2k^2\frac{d^2\tilde{u}_2^a}{dx_2^2} + k^4\tilde{u}_2^a = 0 \tag{11}$$

and

$$\frac{d^4\tilde{u}_2^b}{dx_2^4} - 2k^2\frac{d^2\tilde{u}_2^b}{dx_2^2} + k^4\tilde{u}_2^b = 0. \tag{12}$$

The solution of the above fourth-order ordinary differential equations (ODEs) satisfies the following boundary conditions:

$$\tilde{u}_2^a(x_1,-h) = 0, \quad \sigma_{12}^a(x_1,-h_b) = \sigma_{12}^b(x_1,-h_b),$$

$$\tilde{u}_1^a(x_1,-h) = 0, \quad \sigma_{22}^a(x_1,-h_b) = \sigma_{22}^b(x_1,-h_b),$$

$$\sigma_{12}^b(x_1,0) = 0, \quad \tilde{u}_2^a(x_1,-h_b) = \tilde{u}_2^b(x_1,-h_b),$$

$$\tilde{u}_2^b(x_1,0) = \alpha^b, \quad \tilde{u}_1^a(x_1,-h_b) = \tilde{u}_1^b(x_1,-h_b). \tag{13}$$

The normal elastic stress at the free surface corresponding to the displacement field so obtained can be written as

$$\sigma_{22}^b = 2\mu^b S(kh,M,H)k\alpha^b \cos(kx_1), \tag{14}$$

where M and H are nondimensional numbers defined as

$$M = \frac{\mu^a}{\mu^b} \text{ and } H = \frac{h_b}{h_a + h_b} = \left(\frac{h_b}{h}\right)$$

and S is a dimensionless function (see the Appendix).

By substituting the expression for the normal stress (σ_{22}^b) from Eq. (14) into Eq. (6) and rearranging to a more compact scaled form, the following characteristic equation governing the stability of the system is obtained:

$$\left(\frac{1 + H(M-1)}{M}\right)(kh)S(kh,M,H) = -\frac{Y}{K_{eff}}, \tag{15}$$

where K_{eff} is the effective elastic stiffness of the films defined as

$$K_{eff} = \left(\frac{\frac{\mu^a}{h_a}\frac{\mu^b}{h_b}}{\frac{\mu^a}{h_a} + \frac{\mu^b}{h_b}}\right).$$

The free surface becomes unstable and deforms periodically if for a particular value of the interaction force stiffness Y a real value of the wave number k can be found to satisfy the above equation (15). The minimum value of the adhesive force Y for which the instability of the homogeneous solution occurs is the critical interaction stiffness denoted by Y_c. The wave number that satisfies the Eq. (15) for $Y=Y_c$ is the critical mode of instability (denoted by k_c) which should manifest at the onset of instability as the two surfaces approach each other and the critical adhesive force is achieved.

In case of the single-film asymptotes, which can be obtained by choosing an asymptotic value of the parameters H (0 and 1) and M (1 and ∞), the instability governing relation (15) indeed reduces to the corresponding expressions for the single-film case [4,5,8]:

$$2kh^*\frac{1 + \cosh(2kh^*) + 2(kh^*)^2}{\sinh(2kh^*) - 2kh^*} = -\frac{Yh^*}{\mu^*}, \tag{16}$$

where h^* and μ^* are the thickness and shear modulus of the corresponding effective single film.

Examining expression (15), we observe that the critical wavelength is a function of the total thickness of the bilayer, h, the ratio of thicknesses and the ratio of shear moduli of the two films. Further, as in the case of a single film, the wavelength is again found to be independent of the precise nature and decay of the intermolecular (adhesive) force and also the magnitude of individual shear moduli. The nondimensional quantities M and H in Eq. (15) can range from 0 to ∞ and 0 to 1, respectively. It is thus also useful to define another nondimensional parameter $M_s=M/(1+M)$, which maps M (0 *to* ∞) to M_s (0 *to* 1).

Figure 2 shows the contour plot of the nondimensional critical wavelength (λ_c/h) on an $H-M_s$ plane. The cases with $M_s=0.5$, $H=0$, and $H=1$ correspond to the limit of a single film of thickness h and serve as a reference case represented by the contour line of $\lambda_c/h=2.96$, which is a known result for the case of a single film [4,5,8]. A bilayer with $M_s=1.0$ is another single-film asymptote in which the bottom film of thickness $h(1-H)$ becomes a rigid substrate, so that the wavelength again scales as $2.96hH$ or $2.96h_b$. It is also possible to have $\lambda_c/h=2.96$, which is the scaling corresponding to the single-film case [4,5,8] for cases other than the single-film asymptotes described above. These special contour lines divide the H-M_s plane into four regions. Crossing of these 2.96 level contours results in a change in the stabil-

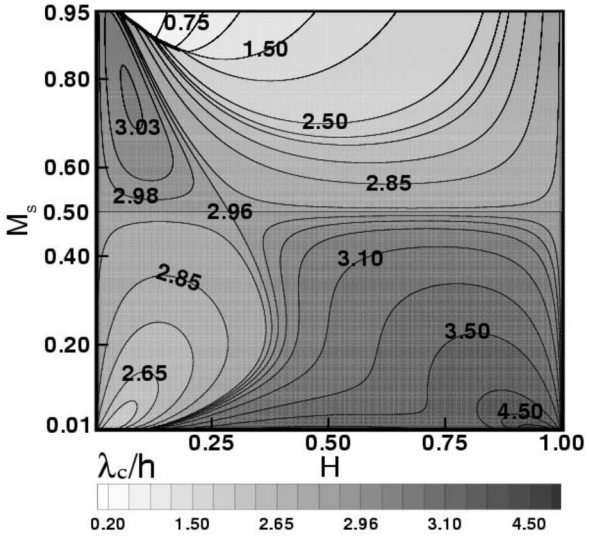

FIG. 2. Contours of λ_c/h on an H-M_s plane.

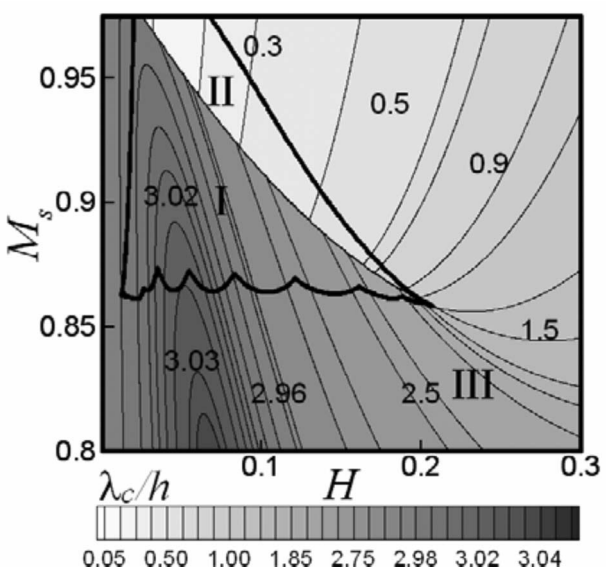

FIG. 3. Close-up view of top left corner of Fig. 2. Regions marked I and II have two minima, one corresponding to a larger wavelength and another to a comparatively shorter wavelength. Systems in region III have one energy minimum (the other one corresponds to a huge energy which can be neglected for the discussions here).

ity characteristics of the bilayers. The top left region in Fig. 2 corresponds to the parameters for which the wavelength scaling is greater than 2.96. It decreases across the 2.96-contour, and above a critical M_s (0.8592 or a critical $M>6.1$), a rather sudden jump down to a low wavelength is found for a particular value of H (H_J). This critical value of H_J decreases with an increase in M_s, and consequently the critical wavelength beyond the jump also becomes shorter. The switch occurs when the compliancy of the bottom film reduces substantially and it almost behaves like a rigid substrate whereas the top layer accommodates most of the deformation. At higher values of M_s, this reduction in compliancy of the bottom layer relative to the top layer occurs at lower values of H and thus lower H_J. In this limit, the wavelength scaling with the top film thickness alone again produces a scaling factor close to 2.96.

Figure 3 shows a magnified view of the left top corner of Fig. 2 with thick dark lines drawn to show the borders of the regions I, II, and III defined below. In regions I and II marked in Fig. 3, two local energy minima of comparable energies coexist. In region III, only a single minimum of the energy exists. When H is increased—namely, when the stiffness of the top film is decreased relative to the bottom film—the energy minimum at the higher wave number becomes deeper. Eventually, it becomes the global minimum of the system, resulting in an abrupt change in the critical wavelength. Beyond a critical value of $H=H_J$, the minimum-energy configuration corresponds to the wavelength dictated by the second deeper minimum. Further, H_J decreases with an increase in M_s. Qualitatively similar predictions were arrived at by Yoon *et al.* [39] by using a different technique namely, Kerr-type analysis. Yoon *et al.* [39] obtained a condition $H/[M(1-H)]>2$, under which the bottom film may effectively be considered to be a rigid substrate and the wavelength scales as $2.96h_b$. We note that this is a rather conservative sufficient condition. The bottom film can in fact be considered rigid where the actual jump in the wavelength takes place as shown by the dark contour in the upper left corner of Fig. 2 and the boundary between regions I and II in Fig. 3. Thus, a shift to the single-film limit can occur even when the condition $H/[M(1-H)]>2$ is not satisfied.

An approximate, but physically motivated analysis, also clarifies the basic idea behind the wave number change. For large values of M, the switching of wavelength occurs when the effective elastic stiffnesses of the two films become comparable: namely, $\mu_1/h_1=\mu_2/h_2$. This condition can be rearranged as $H_J=1/(M+1)$. Based on the full computations from the LSA, we could verify that this is indeed a good approximation to the exact phase boundary where the switch occurs, but only for large values of $M>8$. For example, this approximation predicts $H_J=0.1$ at $M=9.15$, whereas the full LSA prediction is $H_J=0.12$.

This sudden jump in the wavelength corresponding to the minimum critical interaction stiffness also leads to much smaller deformations at the interface between the two films compared to the deformations at the free surface of the top film. Figure 4(a) shows the variation of ratio of amplitudes of the deformation at the two interfaces (α^{ab}/α^{b}), where α^{ab} and α^{b} denote deformation amplitudes normal to the film surface (x_2 direction) at the film-film interface and at the free surface of the top film, respectively. The value of (α^{ab}/α^{b}) is always positive, and thus both interfaces always deform in-phase for all values of M_s and H. The elastic response to any traction is linear. The top film deforms in response to the force and also transmits it to the interface of the buried layer. The buried interface thus deforms in-phase with the top surface. However, the extent of deformation is a function of the shear modulus and thickness of the film. For low values of H—for example, $H=0.025$—α^{ab}/α^{b} remains close to 1 for a wide range of M_s from 0 to close to 1. This implies that the top film maintains its thickness constant by bending uniformly in-phase with the deformations of the more compliant

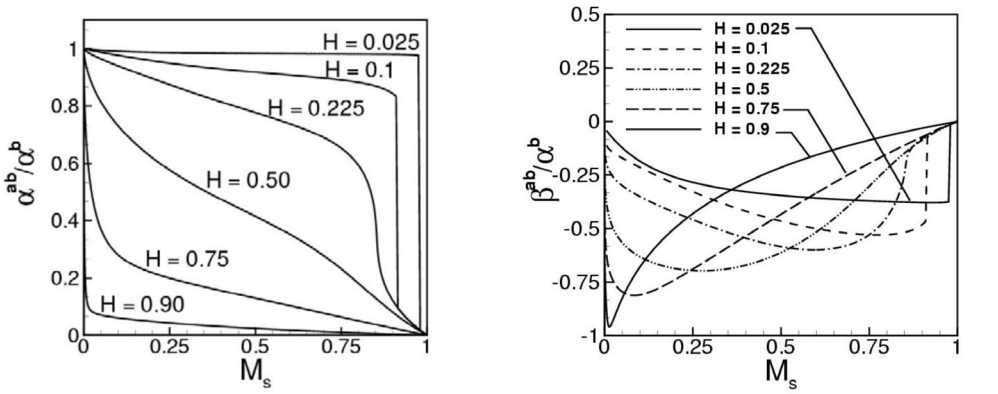

FIG. 4. (a) Variation in α^{ab}/α^b with M_s for different values of H and (b) variation in β^{ab}/α^b with M_s for different values of H.

bottom film a. For $H=0.025$, at $M_s=0.98$, the ratio (~ 0.99) jumps down to a low value (~ 0.13), implying that the bottom layer can now be assumed to be a nearly undeformed rigid substrate when $M_s > 0.98$. This critical M_s, at which a jump in (α^{ab}/α^b) occurs, increases with a decrease in H and, in fact, no jump is observed below $M_s < 0.86$ (i.e., $M < 6.1$). For $H > 0.225$, α^{ab}/α^b decreases rapidly with an increase in M_s. With an increase in H, the compliance of the bottom film reduces and the ratio α^{ab}/α^b decreases sharply at small values of M_s.

A softer film of smaller shear modulus μ at the bottom ($M_s < 0.5$) is expected to accommodate more deformations than the higher-modulus surface layer. In addition, the thicker of the two films can be deformed more because of its increased compliance, h/μ. Thus, if the softer bottom film is thicker, we observe a decrease in the nondimensional wavelength (λ_c/h) as compared to that obtained for the single film case (see Fig. 2).

For $M_s < 0.5$ and low values of H, the critical wavelength when scaled with the total thickness shows a decrease below the single-film case value of $2.96h$ (Fig. 2), but scaling with the thickness of the bottom film alone increases the scaling factor (λ_c/h^a) close to that of the single film. The top layer in this case merely bends in response to the deformations in the bottom film. The latter in this case governs the stability of the bilayer because of it being a highly compliant film. The top film merely transfers the stresses on its free surface to the film-film interface ab. The maximum value of the scaling factor Sc_h (λ_c/h) increases with decrease in M_s and the corresponding H also increases. For $M_s=0.25$ and $H=0.80$, $\mathrm{Sc}_h=3.5$, whereas for $M_s=0.01$ and $H=0.94$, $\mathrm{Sc}_h=5.6$. This is much higher than the single-film scaling factor: namely, 2.96. This increase in the wavelength can be attributed to the large deformation in the x_1 direction at the film-film interface as the bottom layer is much softer and thus accommodates much more deformation in the x_1 direction [Fig. 4(b)], but not in the x_2 direction due to reduced compliance as shown in Fig. 4(a). In Fig. 4(b), the curve for $H=0.9$ indeed shows a substantial increase in β^{ab}/α^b (β^{ab} is the amplitude of the sinusoidal displacement of the common interface in the x_1 direction) for lower values of M_s. The top film in such cases has an effective sliplike behavior because of a very soft and very thin film below it in which the shear deformation is dominant. The wavelength is thus increased. With an increase in M_s, this effect reduces because of less deformation (both horizontal and vertical) in the bottom film and asymptotically reduces to zero at $M_s=1$. Consequently, the scaling factor also decreases with increase in M_s (Fig. 2).

IV. SIMULATIONS OF DEBONDING BY CONTACTOR PULL-OFF: WAVELENGTHS, DEFORMATIONS, AND ADHESIVE CONTACT AREAS

In purely elastic films, the morphology of a film is governed by the minimum-energy configurations. The energy of a bilayer film system is comprised of the elastic stored energies of the two films and the energy of interaction of the top surface with the contactor. The surface energy contributions have been neglected as it is not significant unless the films are submicrometer [5,8].

The volume integral over the stored elastic energy [Eq. (2)] can be reduced to a surface integral as

$$\int_V W(\varepsilon)dV = \frac{1}{2}\int_{S^b} \sigma_{22}u_2 dS^b, \tag{17}$$

where S^b denotes the free surface of the bilayer film.

Deformations of the free surface of the bilayer in the x_2 direction can be expanded in the form of a Fourier series as

$$u_2^b = \sum_{n=0}^{N-1} a_n \cos(k_n x_1), \tag{18}$$

where a_n's are the Fourier coefficients for the deformation of the free interface and k_n's are the corresponding wave numbers defined by $k_n = 2n\pi/L$, where L is the x domain of simulation. We choose L to be $32h$ in our simulations and retain 128 Fourier modes ($n=1-128$). This decomposition can resolve the modes an order of magnitude smaller and larger than the dominant wavelength.

The total potential energy per unit width in terms of the Fourier components of deformation of the film surface can be written as [11,12]

$$\Pi(a_0,a_1,a_2,\ldots,a_{N-1}) = \frac{\pi\mu L}{2}\sum_{n=0}^{N-1} n a_n^2 k_n S(k_n h, M, H) - \int_{S^b} U\left(d - \sum_{n=0}^{N-1} a_n \cos(k_n x_1)\right) dx_1, \tag{19}$$

where $L \gg \lambda$ is the length of the domain.

In the simulations shown here, we employ a standard Lennard-Jones interaction potential composed of the van der Waals attraction with a short-range repulsion [8,41–44]. The potential thus depends upon the local separation distance between the film free surface and the contactor:

$$U(d-\boldsymbol{u}^b\cdot\boldsymbol{n}) = -\frac{1}{12\pi}\frac{A}{(d-\boldsymbol{u}^b\cdot\boldsymbol{n})^2} + \frac{B}{(d-\boldsymbol{u}^b\cdot\boldsymbol{n})^8}. \quad (20)$$

Coefficients A and B denote the Hamaker constant and the Born repulsion coefficient, respectively [8,11,12,42–44]. The Hamaker constant depends on the materials of the interacting surfaces, and its magnitude reflects the strength of the van der Waals attractive interactions. The Born repulsion coefficient B can be determined using the equilibrium condition $\partial U(d)/\partial d=0$ at an equilibrium separation distance d_e $=0.158$ nm, which is found to be a constant nearly independent of the materials [41–44]. Here d_e is the equilibrium distance below which the contactor-film surface interaction is repulsive due to the short-range electronic orbital overlap. The Hamaker constant A ($\sim 10^{-19}$–10^{-21} J) thus also determines the adhesion energy per unit area between the bilayer surface and the contactor by the relation $\Delta G = U(d_e)$. We choose here a realistic magnitude of the Hamaker constant, $A=10^{-20}$ J [15,41–44]. This essentially means that we focus on the effects of elastic stiffness and thickness (M and H) by keeping the adhesion energy constant. The results for other values of adhesive energy (not shown) are qualitatively similar and present no new physics.

The Fourier coefficients (a_n's) are obtained by minimizing the energy [Eq. (18)] of the system by using a conjugate gradient algorithm [11,12]. The contactor was initially placed at a separation distance slightly smaller ($\sim 0.90 d_c$) than the critical separation distance d_c from the linear analysis at the onset of instability. The contactor is then moved farther from the film (peeling mode [11,12]) in small steps s. A small initial random perturbation is imparted to the free surface in order to sample the nearest local minimum of the total energy more effectively. The wavelength of the patterns obtained through simulations when the contactor is below the critical separation distance is in agreement with the predicted value from the linear analysis. The Fourier coefficients from the previous configuration were used as the initial guess for the conjugate gradient scheme to simulate the stepwise peeling. The deformations at the film-film interface are a function of the deformation in the free surface and can be obtained using the summation over the solution obtained in Sec. III. Simulations have been performed under small strain approximation. Geometric nonlinearities in the debonding sequence are small as the aspect ratio of the maximum deformation to the thickness of the film is small (~ 0.01).

Figure 5 shows the changes in the morphology with the contactor pull-off obtained for a bilayer film with $M=6.0$ and $H=0.5$. The other dimensional parameters describing the film properties are the shear modulus $\mu^b=10$ MPa and the thickness of film b, $h_b=5$ μm. The contactor is pulled away from the films in steps of 1.0 nm, and a minimum-energy configuration is obtained at each step. The film surface first jumps in contact with the approaching contactor at $\sim d_c$ and

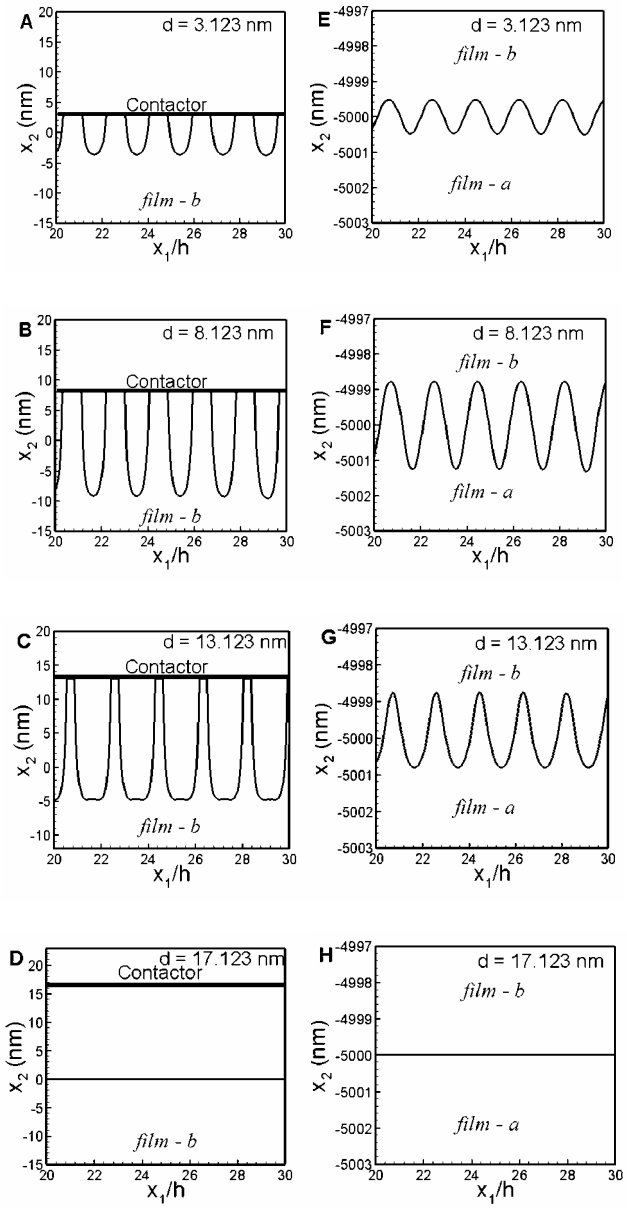

FIG. 5. Debonding of a bilayer film by contactor pull-off. $M=6.0$ and $H=0.5$. The shear modulus of the top film is 10 MPa, and the thickness of the top film is 5 μm.

forms a periodic columnar structure of a wavelength ($kh=3.33$) that is in agreement with the linear analysis ($kh=3.35$). As the contactor is retracted away in small steps ($s<1$ nm), the columns grow in height and progressively become slender [Figs. 5(b) and 5(c)]. For the first few steps, the columns continue to adhere to the contactor with the same contact area (pinning mode [11]), but after a certain separation distance, they undergo thinning of their cross sections by peeling at the edges. This observation matches with the debonding sequence in the single-film case [11,12]. The columns are separated by the same wavelength with which the patterns were formed during the first step of adhesion. With the thinning of the columns at larger distances, elastic stresses in the film increase at the column edges, leading to a snap-off

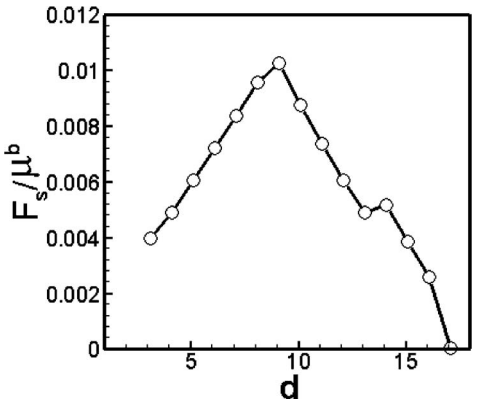

FIG. 6. Variation in the force, required by the contactor to hold the film, with the separation distance for a bilayer film with $M=6.0$ and $H=0.5$.

of the columns from the contactor, and the film eventually regains planarity at some debonding distance. The separation distance at which the columns [Fig. 5(d)] snap off is much larger than the distance at which the onset of contact instability takes place. This is because of the metastability and persistence of the local minimum-energy states as discussed previously [11,12]. Figures 5(e)–5(h) show the film-film interface *ab* corresponding to the free-surface configurations given in Figs. 5(a)–5(d) respectively. As expected for a stiffer bottom layer, the amplitude of deformation of the film-film interface relative to the free-surface deformation is indeed observed to be much smaller. Another observation is that the free-surface and film-film interface always deforms in phase and the squeezing mode of instability is always absent because of its high elastic energy penalty.

It is interesting to consider the reasons for the invariance of the pattern length scale even in the nonlinear regime away from the onset of instability. The underlying physics of this phenomenon is addressed in the context of a single film elsewhere, both theoretically and experimentally [8,11,12,15]. Basically, after the onset of instability, the formation of adhesive contacts locks in the wavelength in a local metastable energy minimum. Thus, even though the resulting surface shape is clearly not sinusoidal anymore, the dominant wavelength cannot and does not change much until the existing columns, which are already in adhesive contact, can collapse.

Figure 6 shows variation of the external force per unit area (F_s) required for the contactor to hold the film in equilibrium [$F_s=\int_0^L \sigma_{22}(x_1,0)dx_1/L$] at a separation distance d. During the pinned phase of contactor retraction, the force F_s rises linearly as expected from a linear stretching of the columns without any change in their cross section. At the onset of the peeling mode of adhesive failure, the force declines with a further increase in d. Beyond the maximum pull-off force, the contact area reduces and columns become progressively slender. The kink in Fig. 6 during the peeling mode represents an intermittent pinning of the film in one of the debonding steps due to the existence of multiple minima with very close energies. This has also been observed in the debonding process of a single film [8].

V. CONCLUSIONS

The analysis of stability of bilayer films in a vertically confined geometry reveals several interesting aspects of adhesion and debonding at soft interfaces. The asymptotic case of a single elastic film is readily recovered from our analysis of a bilayer when either of the two thicknesses vanish or when both the films have the same shear modulus. The key findings of the study are the following.

(i) Surfaces of a bilayer film undergo inhomogeneous deformations when the adhesive interactions with the contactor exceed a critical force or, in other words, when the intersurface distance is less than a critical distance. The wavelength of the contact instability at the critical force does not depend upon the nature or strength of the interaction force and is a function only of the total thickness of the films, their thickness ratio, and shear moduli ratio. This provides a greater control of the pattern length scale in contrast to a single film where pattern wavelength is proportional to film thickness alone.

(ii) When the bottom film of a bilayer is softer, a jump in the wavelength is observed beyond a shear modulus ratio ($M>6.1$) and a threshold thickness ratio H_J—for example, $H_J=0.20$ for $M=6.1$. For a thickness ratio below H_J the instability is governed largely by the more compliant bottom film, but beyond H_J, it is governed by the top film thickness and bottom film behaves much like a rigid substrate.

(iii) When the bottom film is much softer ($M<0.01$), much longer wavelengths ($>4h-8h$) compared to a single film are observed for $H>0.25$ and especially near $H=1$. The peak in the wavelength near $H=1$ of Fig. 4(b) indicates that the much thinner and softer bottom film in this case accommodates much more deformation in the horizontal direction and thus imitates a sliplike effect for the top film, leading to longer wavelengths.

(iv) Non linear simulations based on energy minimization during the processes of initial adhesion and debonding are in agreement with the predictions of the linear stability analysis for the critical force and the wavelength. The debonding sequence is made up of the initial pinning of the columns followed by their sideways peeling at a maximum force. This is similar to the debonding sequence in a single film [11,12]. However, the wavelength of the patterns formed, critical separation distance, and the force-distance curves are significantly different from the case of a single film.

In view of the above points, we note that a bilayer film configuration provides far greater control of the pattern length scale than in the case of a single film. Both shorter (down to $0.5h$) and longer wavelengths (up to $8h$) can be obtained. This is in contrast to the case of the single film where the pattern wavelength is always $3h$. Variation of the shear modulus across the film thickness provides a tool to modify the instability length scale, debonding distance, and pull-off force, as well the strength of the adhesive force required to initiate the instability. In particular, the use of a bilayer affords substantial miniaturization of patterns formed by the elastic contact instability below the $3h$ limit of a single film. This has direct implications for elastic contact lithography proposed recently [14].

ACKNOWLEDGMENTS

We thank M. K. Chaudhury and A. Ghatak for illuminating discussions over the years on elastic layers. The work was supported by the DST Unit on Nanosciences at IIT Kanpur. V.S. also thanks DST for support through the Nanoscience program. A.S. acknowledges support from the DST.

APPENDIX

The characteristic equation (Eq (15) in Sec. III) governing the stability of the bilayer elastic film is written in terms of a dimensionless function $S(kh,M,H)$ given by,

$$
\begin{aligned}
S(kh,M,H) = [&- (e^{4kh}(-1+M)^2 + e^{2Hkh}(-1+M)^2 + e^{4Hkh}(1 \\
&+ M)^2 + e^{4(1+H)kh}(1+M)^2 + 2e^{2(1+H)kh}[1 + 2(\\
&- 1+H)^2(kh)^2](-1+M^2) + 2e^{2(1+3H)kh}[1 + 2(\\
&- 1+H)^2(kh)^2](-1+M^2) + 2e^{6Hkh}[1 \\
&+ 2H^2(kh)^2](-1+M^2) + 2e^{2(2+H)kh}[1 \\
&+ 2H^2(kh)^2](-1+M^2) + 4e^{2(1+2H)kh}\{1 + 4(-1 \\
&+ H)^2H^2(kh)^4(-1+M)^2 + M^2 + 2(kh)^2[1 - 2H(\\
&- 1+M)^2 + 2H^2(-1+M)^2 + M^2]\})]/\{e^{4kh}(-1 \\
&+ M)^2 - e^{2Hkh}(-1+M)^2 + e^{4Hkh}(1+M)^2 \\
&- e^{4(1+H)kh}(1+M)^2 + 8e^{2(1+2H)kh}kh[-4H^2(kh)^2(\\
&- 1+M)^2 + 2H^3(kh)^2(-1+M)^2 + H(1 \\
&+ 2(kh)^2](-1+M)^2 + 2M) + 4e^{6Hkh}Hkh(-1 \\
&+ M^2) + 4e^{2(2+H)kh}Hkh(-1+M^2) + 2e^{2(1+H)kh}[1 \\
&+ 2(-1+H)^2(kh)^2](-1+M^2) - 2e^{2(1+3H)kh}[1 \\
&+ 2(-1+H)^2(kh)^2](-1+M^2)\}. \qquad \text{(A1)}
\end{aligned}
$$

[1] K. R. Shull, C. M. Flanigan, and A. J. Crosby, Phys. Rev. Lett. **84**, 3057 (2000).
[2] A. Ghatak, M. K. Chaudhury, V. Shenoy, and A. Sharma, Phys. Rev. Lett. **85**, 4329 (2000).
[3] W. Monch and S. Herminghaus, Europhys. Lett. **53**, 525 (2001).
[4] V. Shenoy and A. Sharma, Phys. Rev. Lett. **86**, 119 (2001).
[5] V. Shenoy and A. Sharma, J. Mech. Phys. Solids **50**, 1155 (2002).
[6] V. Shenoy and A. Sharma, J. Appl. Phys. **94**, 6376 (2003).
[7] A. Ghatak and M. K. Chaudhary, Langmuir **19**, 2621 (2003).
[8] J. Sarkar, V. Shenoy, and A. Sharma, Phys. Rev. Lett. **93**, 018302 (2004).
[9] C. Q. Ru, J. Appl. Mech. **71**, 138 (2004).
[10] A. Ghatak, L. Mahadevan, J. Y. Chung, M. K. Chaudhary, and V. Shenoy, Proc. R. Soc. London, Ser. A **460**, 2725 (2004).
[11] J. Sarkar, A. Sharma, and V. Shenoy, Langmuir **21**, 1457 (2005).
[12] J. Sarkar, A. Sharma, and V. Shenoy, J. Adhes. **81**, 271 (2005).
[13] Shi-Qing Huang, Qun-Yang Li, Xi-Qiao Feng, and Shou-Wen Yu, J. Mech. Mater. **38**, 88 (2006).
[14] M. Gonugutala, A. Sharma, R. Mukherjee, and S. A. Subramanian, Langmuir **22**, 7066 (2006).
[15] M. Gonuguntla, A. Sharma, J. Sarkar, S. A. Subramanian, M. Ghosh, and V. Shenoy, Phys. Rev. Lett. **97**, 018303 (2006).
[16] L. H. He and C. W. Lim, Int. J. Solids Struct. **43**, 132 (2006).
[17] N. Arun, A. Sharma, V. Shenoy, and K. S. Narayan, Adv. Mater. (Weinheim, Ger.) **18**, 660 (2006).
[18] G. Reiter, Phys. Rev. Lett. **68**, 75 (1992).
[19] A. Oron, S. H. Davis, and S. G. Bankoff, Rev. Mod. Phys. **69**, 931 (1997).
[20] S. Herminghaus, K. Jacobs, K. Mecke, J. Bischof, A. Fery, M. Ibn-Elhaj, and S. Schlagowski, Science **282**, 916 (1998).
[21] E. Schaffer, T. Thurn-Albrecht, T. P. Russel, and U. Steiner, Nature (London) **403**, 874 (2000).
[22] A. Sharma, Eur. Phys. J. E **12**, 397 (2003).
[23] A. Sharma and K. Kargupta, Appl. Phys. Lett. **83**, 3549 (2003).
[24] S. Kumar and O. K. Matar, J. Colloid Interface Sci. **273**, 581 (2004).
[25] P. J. Yoo, K. Y. Suh, S. Y. Park, and H. H. Lee, Adv. Mater. (Weinheim, Ger.) **14**, 1383 (2002).
[26] R. Huang and Z. Suo, J. Appl. Phys. **91**, 1135 (2002).
[27] S. J. Kwon, J. H. Park, and J. G. Park, Phys. Rev. E **71**, 011604 (2005).
[28] S. Kumar, Langmuir **19**, 2473 (2003).
[29] A. A. Golovin, M. S. Levine, T. V. Savina, and S. H. Davis, Phys. Rev. B **70**, 235342 (2004); A. A. Golovin, S. H. Davis, and P. W. Voorhees, Phys. Rev. E **68**, 056203 (2003).
[30] C. Y. Hui, N. J. Glassmaker, T. Tang, and A. Jagota, J. R. Soc., Interface **1**, 35 (2004).
[31] J. Y. Chung and M. K. Chaudhary, J. R. Soc., Interface **2**, 55 (2005).
[32] W. Tsukruk, H. S. Ahn, D. Kim, and A. Sidorenko, Appl. Phys. Lett. **80**, 4825 (2002).
[33] B. Bhushan and W. Peng, Appl. Mech. Rev. **55**, 435 (2002).
[34] J. Y. Chung and M. K. Chaudhary, J. Adhes. **81**, 1119 (2005).
[35] C. Q. Ru, J. Appl. Phys. **90**, 6098 (2001).
[36] V. Shenoy and A. Sharma, Langmuir **18**, 2216 (2002).
[37] J. Sarkar, V. Shenoy, and A. Sharma, Phys. Rev. E **67**, 031607 (2003).
[38] J. Y. Chung, K. Kim, M. K. Chaudhary, J. Sarkar, and A. Sharma, Eur. Phys. J. E **20**, 47 (2006).
[39] J. Yoon, C. Q. Ru, and A. Midouchowski, J. Appl. Phys. **98**, 113503 (2005).
[40] A. D. Kerr, Ing.-Arch. **54**, 455 (1984).
[41] J. Israelachvili, *Intermolecular and Surface Forces* (Academic, San Diego, CA, 1992).
[42] J. C. van Oss, M. K. Chaudhary, and R. J. Good, Chem. Rev. (Washington, D.C.) **88**, 927 (1988); A. Ghatak, R. Khanna, and A. Sharma, J. Colloid Interface Sci. **212**, 483 (1999).
[43] V. S. Mitlin and N. V. Petviashvili, Phys. Lett. A **192**, 323 (1994).
[44] A. Sharma and R. Khanna, Phys. Rev. Lett. **81**, 3463 (1998).